

# PhysioSync: Temporal and Cross-Modal Contrastive Learning Inspired by Physiological Synchronization for EEG-Based Emotion Recognition

Kai Cui<sup>†</sup>, Jia Li<sup>†\*</sup>, Yu Liu<sup>\*</sup>, Xuesong Zhang, Zhenzhen Hu, Meng Wang, *Fellow, IEEE*

**Abstract**—Electroencephalography (EEG) signals provide a promising and involuntary reflection of brain activity related to emotional states, offering significant advantages over behavioral cues like facial expressions. However, EEG signals are often noisy, affected by artifacts, and vary across individuals, complicating emotion recognition. While multimodal approaches have used Peripheral Physiological Signals (PPS) like GSR to complement EEG, they often overlook the dynamic synchronization and consistent semantics between the modalities. Additionally, the temporal dynamics of emotional fluctuations across different time resolutions in PPS remain underexplored. To address these challenges, we propose PhysioSync, a novel pre-training framework leveraging temporal and cross-modal contrastive learning, inspired by physiological synchronization phenomena. PhysioSync incorporates Cross-Modal Consistency Alignment (CM-CA) to model dynamic relationships between EEG and complementary PPS, enabling emotion-related synchronizations across modalities. Besides, it introduces Long- and Short-Term Temporal Contrastive Learning (LS-TCL) to capture emotional synchronization at different temporal resolutions within modalities. After pre-training, cross-resolution and cross-modal features are hierarchically fused and fine-tuned to enhance emotion recognition. Experiments on DEAP and DREAMER datasets demonstrate PhysioSync’s advanced performance under uni-modal and cross-modal conditions, highlighting its effectiveness for EEG-centered emotion recognition. The source code will be publicly available at <https://github.com/MSA-LMC/PhysioSync>.

**Index Terms**—EEG-based emotion recognition, multi-modal fusion, contrastive-learning.

## I. INTRODUCTION

RECOGNIZING emotional states through physiological signals is a critical yet challenging task in human-computer interaction, disease diagnosis, and rehabilitation, attracting substantial research attention recently [1]–[5]. Compared to facial expressions, EEG stands out as a non-invasive, cost-effective modality with high temporal resolution, offering direct and involuntary reflections of emotional states, thus establishing itself as the cornerstone of emotion recognition research [6]–[11]. Despite its advantages, EEG-based emotion recognition faces challenges such as overfitting to noise from

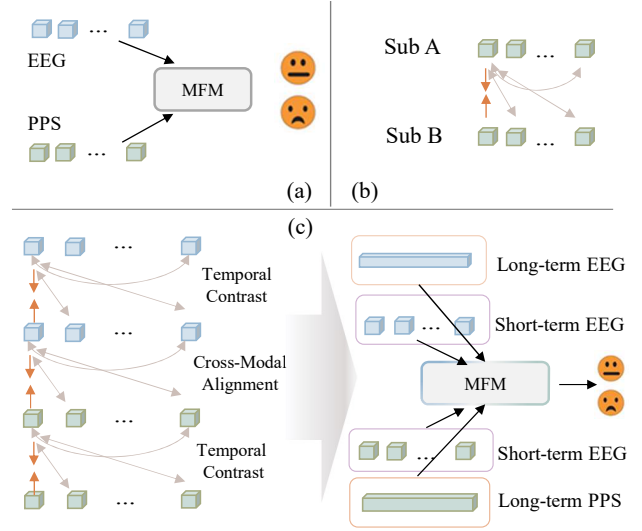


Fig. 1. Overview of the proposed approach compared to existing methods. (a) represents the simple combination of EEG and peripheral physiological signals (PPS) (w/o pre-training); (b) involves contrastive learning (w/ pre-training); (c) represents our method (w/ pre-training). Orange arrows denote positive pairs, while gray arrows indicate negative pairs. MFM refers to the modality fusion module.

physiological artifacts and insensitivity to inter-subject variability [12], which recent studies [13]–[17] suggest can be mitigated by incorporating Peripheral Physiological Signals (PPS) to provide complementary information. Notably, some studies suggest that EEG is better for predicting arousal, while PPS are more suited for assessing valence [18], highlighting the benefit of integrating both. Nevertheless, from the perspective of physiological synchronization, incorporating complementary signals does not fully address the challenges of cross-subject variability and may even worsen modal heterogeneity, presenting a significant barrier to the advancement of multimodal emotion recognition.

To address these challenges, current research efforts are primarily focused on multi-modality heterogeneity and cross-subject divergence. Some approaches combine EEG with Peripheral Physiological Signals (PPS) (Fig. 1 (a)). For example, Zhu et al. [16] introduced facial expressions in conjunction with EEG signals for dynamic, confidence-aware multimodal fusion and prediction. Similarly, Fu et al. [17] proposed a cross-modal guiding neural network, utilizing EEG features to guide the extraction of eye movement features, thereby

<sup>†</sup> Equal contribution. <sup>\*</sup> Corresponding authors.

Kai Cui, Yu Liu are with the School of Instrument Science and Optoelectronics Engineering, Hefei University of Technology, Hefei 230009, China (e-mail: kaic@mail.hfut.edu.cn; yuliu@hfut.edu.cn).

Jia Li, Xuesong Zhang, Zhenzhen Hu, Meng Wang are with the School of Computer Science and Information Engineering, Hefei University of Technology, Hefei 230009, China (e-mail: jiali@hfut.edu.cn; xszhang\_hfut@mail.hfut.edu.cn; zzhu@hfut.edu.cn; eric.mengwang@gmail.com).

mitigating the impact of subjective factors. These studies underscore the value of PPS as supplementary information to EEG. However, there is a notable gap in research concerning consistent semantic alignment between different modalities and EEG signals to overcome multi-modal heterogeneity. For effective multimodal emotion recognition, it is essential that signals from different modalities are semantically aligned [19]. Intuitively, signals from different modalities should be correlated when exposed to the same emotional stimuli. In addition to multi-modal heterogeneity, cross-subject variability continues to be a pervasive challenge. To tackle this, recent studies have employed contrastive learning to learn spatiotemporal representations that align EEG signals across subjects (Fig. 1 (b)). For example, Shen et al. [20] utilized convolutional neural networks to align EEG features across subjects using contrastive learning. However, these methods typically apply contrastive learning at a single temporal resolution, while emotional fluctuations inherently involve both short-term and long-term correlations [21].

In this paper, we tackle the heterogeneity between complementary PPS and EEG signals, as well as cross-subject variability, through cross-modal alignment and contrastive learning. Additionally, we capture the dynamic characteristics of emotion by extracting and integrating features across multiple temporal scales. Specifically, we propose a contrastive learning framework for physiological synchronization that integrates EEG with PPS (Fig. 1 (c)).

Our contrastive learning framework includes two key components: To minimize discrepancies in physiological signals induced by the same emotional stimulus across subjects, we propose TCL (intra-modal temporal contrastive learning). To align signals from different modalities in a shared semantic space, we introduce CM-CL (cross-modal contrastive learning). This dual branch facilitates intra-modality temporal synchronization for feature extraction, alongside inter-modality synchronization and interaction. Encoders that extract long-term and short-term features are pre-trained separately based on the different resolutions of the input signal. In the fine-tuning stage, long-term physiological signals are decomposed into short-term segments, which are then processed by the pre-trained encoders to extract both long-term and short-term features, capturing the temporal dynamics of emotional states and offering a comprehensive perspective for emotion recognition.

Specifically, our contributions are as follows:

- A temporal and cross-modal contrastive learning framework, inspired by physiological synchronization phenomena, is proposed to pre-train emotional representations in time domain. It aligns features intra- and inter-modal within same stimulus segments, capturing consistent emotional patterns across physiological signals.
- We pre-train representations on different temporal windows (e.g., 1-second and 5-second windows) for EEG and PPS, effectively modeling short- and long-term emotional dynamics. During fine-tuning, fusing features across temporal resolutions and modalities significantly improves emotion recognition accuracy.

- Our method directly processes raw EEG and PPS as temporal sequences using a Transformer-based backbone, eliminating the need for handcrafted features like differential entropy, and providing a simple, reproducible baseline for future research in EEG-based emotion recognition.

## II. RELATED WORK

### A. EEG-Based Multimodal Emotion Recognition

Electroencephalographic (EEG) signals, reflecting brain activity and psychological processes, contain vital psychophysiological information [4]. Unlike other physiological signals, EEG is directly tied to the central nervous system, offering more precise emotional insights [22]. This advantage has driven the development of various EEG-based emotion recognition methods [23], [24]. However, many methods still rely on hand-crafted features like power spectral density (PSD) and differential entropy (DE), rather than fully exploiting the potential of deep learning models. In contrast, some approaches use raw EEG data with advanced techniques like CNNs and LSTMs to capture spatial and temporal features. For instance, Yin et al. [25] proposed a framework combining graph CNNs and LSTMs, while Ding et al. [26] introduced TSception, a multi-scale CNN that integrates dynamic temporal, asymmetric spatial, and high-level fusion layers for more effective representation learning across temporal and channel dimensions.

Despite these advancements, the complexity of human emotional states poses a significant challenge. A single EEG modality is insufficient to provide a comprehensive representation of the current emotional state, and achieving satisfactory recognition in terms of both accuracy and robustness remains a challenge [27]. To address this, researchers have explored methods that combine signals from the central nervous system [28] (e.g., EEG) and the peripheral nervous system [29] (e.g., GSR, ECG, EMG, EOG, etc.). Jimenez et al. [30] proposed a multi-modal and multi-source Domain Adaptation (MDA) method for addressing the multi-modal emotion recognition problem using EEG and eye movement signals. Li et al. [31] presented a fusion model that leverages the Cross Modal Transformer (CMT), Low Rank Fusion (LRF), and modified CMT (MCMT) to reduce incongruity and redundancy among multimodal physiological signals.

### B. Contrastive Learning for Physiological Representation

Contrastive learning is a form of self-supervised learning that aims to learn representations without relying on manual labels. It has demonstrated state-of-the-art performance across various domains, including computer vision (CV) [32], natural language processing (NLP) [33], and bioinformatics [34]. Typically, contrastive learning methods involve pre-training representations on relatively large datasets, which are then fine-tuned for downstream tasks [35]. However, in the domain of physiological signal emotion recognition, particularly in Electroencephalogram (EEG)-based emotion recognition, the absence of large-scale datasets presents a significant challenge for pre-training. To address this, Shen et al. [20] proposed a

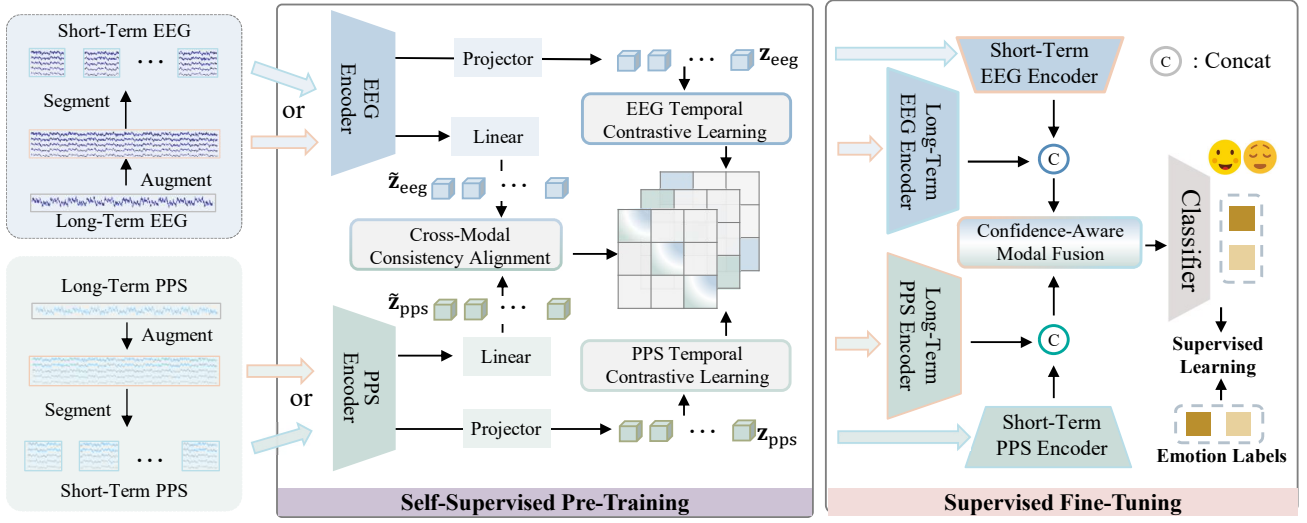


Fig. 2. The proposed a Contrastive Learning framework for Physiological Synchronization, which consists of a self-supervised pre-training phase and a supervised fine-tuning phase. Fig. 3 provides the details of the Encoder and Projector. Fig. 4 illustrates the Fusion Module and Classifier.

contrastive learning strategy tailored for cross-subject generalization. This approach learns the similarities between samples from different subjects exposed to the same stimuli, enabling the model to generalize across subjects. Notably, their method does not rely on large external datasets; instead, it generates numerous self-supervised labels based on the alignment of experimental designs across subjects.

One form of contrastive learning involves classifying samples into positive and negative pairs based on the internal relationships within the data. Using a specific loss function, this approach aims to maximize the similarity between positive pairs while minimizing the similarity between negative pairs [32]. Kan et al. [36] utilized self-supervised learning alongside a novel genetics-inspired data augmentation method to achieve state-of-the-art performance in EEG-based emotion recognition. Simultaneously, contrastive learning methods have also been introduced in cross-corpus EEG-based emotion recognition. Liu et al. [37] introduced a cross-domain contrastive learning strategy during the pre-training phase and incorporating inter-electrode structural connectivity during the fine-tuning phase, the method significantly improved the accuracy of emotion recognition across different datasets. Our work introduces a multi-modal contrastive learning approach that effectively integrates both temporal and cross-modal contrastive learning to better combine multi-modal information.

### III. PROPOSED METHOD

This section introduces PhysioSync, a novel contrastive learning framework with two phases: self-supervised pre-training and supervised fine-tuning (Fig. 2). Section A covers the data input and augmentation for multimodal physiological signals. Section B presents the temporal and cross-modal contrastive optimization mechanism. Section C describes the fine-tuning strategy, aligning pre-trained features with emotion labels through task-specific layers.

#### A. Preliminaries

1) *Long- and Short-term Clip Segmentation*: To capture multi-scale emotional features, we set different time lengths of  $t$  to train encoders for long-term and short-term feature extraction, respectively. Specifically, the input is processed in mini-batches from subjects A and B as an example, the data from each trial of subject A is divided into  $t$ -second clips in temporal order, resulting in  $N$  clips denoted as  $\mathbf{X}_{i,A}^{\text{eeg}}$  ( $i = 1, 2, 3, \dots, N$ ), where  $\mathbf{X}_{i,A}^{\text{eeg}} \in \mathbb{R}^{C \times S}$ ,  $C$  is the number of channels, and  $S$  is the number of sampling points. Similarly, subject B's eeg data is divided into  $\mathbf{X}_{i,B}^{\text{eeg}}$  ( $i = 1, 2, 3, \dots, N$ ). segments  $\mathbf{X}_{i,A}^{\text{eeg}}$  and  $\mathbf{X}_{i,B}^{\text{eeg}}$  from the same video stimulus form a positive pair, while  $\mathbf{X}_{i,S}^{\text{eeg}}$  and  $\mathbf{X}_{j,S}^{\text{eeg}}$  ( $j \neq i, S \in \{A, B\}$ ) from different video stimuli form a negative pair. For all subjects and other modalities, such segmentation is performed, then segments for  $K$  video stimuli from 2 subjects are randomly sampled to form a mini-batch  $\mathbf{G}_m = \{\mathbf{X}_{i,S}^m \mid i = 1, 2, 3, \dots, K; S \in \{A, B\}\}$  as input for pre-training. Here,  $m$  can represent both eeg or pps.

2) *Data Augmentation*: A major challenge in using physiological signals for emotion recognition is the limited number of subjects and small public datasets, which can hinder model training [38]. To address this, data augmentation techniques, such as scaling and noise addition, can be employed to expand the dataset [39], [40], and introduce more positive samples for contrastive learning. The data augmentation step generates more training samples and improves emotion-related semantic consistency learning against moderate noise. Specifically, two scaling factors are applied to the original samples, and Gaussian noise with a fixed mean and signal-to-noise ratio (SNR) is added. The process can be summarized as follows:

$$\tilde{\mathbf{G}}_m = \mathcal{A}(\mathbf{G}_m), \quad (1)$$

where  $\mathcal{A}$  represents the data augmentation operation. Through scaling, noise addition, and their combination, the data is

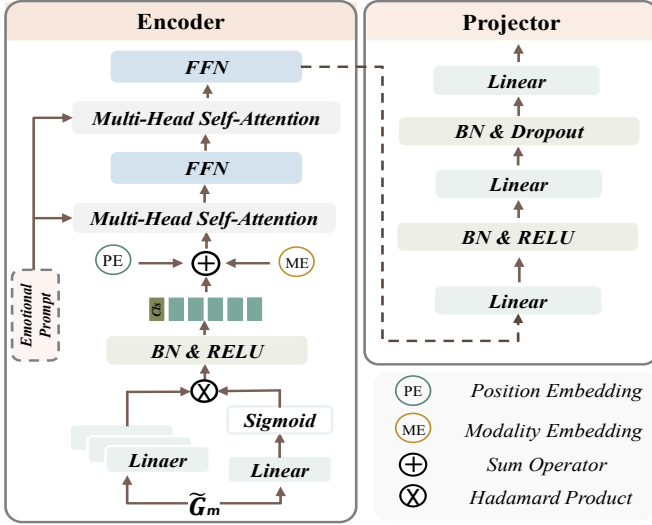


Fig. 3. The illustration of Encoder and Projector, where the Encoder we take part of the structure from [3].

augmented to five times its original size. Finally, the input can be represented as:

$$\tilde{\mathbf{G}}_m = \{\tilde{\mathbf{X}}_{i,S}^m | i = 1, 2, 3, \dots, 5K; S \in \{A, B\}\}. \quad (2)$$

### B. Self-supervised Pre-training Strategy

1) *Pretraining model*: Previous work has shown that self-supervised pre-training strategies can significantly aid model learning. Building upon the structure from [3], we have designed an encoder, as illustrated in Fig. 3.

Physiological signals are input and transformed into  $z$  embeddings through parallel linear layers, aiming to encourage the model to focus on different views of features. Another linear layer followed by an activation function is used to gate the embeddings with information useful for emotion recognition. Subsequently,  $\mathbf{E}_i$  and  $\tilde{\mathbf{E}}$  are multiplied element-wise and aggregated across the  $z$  embeddings to obtain  $\mathbf{e} = (e_1, \dots, e_z)$ . The formula is as follows [3]:

$$\mathbf{E}_i = \text{Linear}_i(\tilde{\mathbf{G}}_m), \quad i = 1, \dots, z, \quad (3)$$

$$\tilde{\mathbf{E}} = \sigma(\text{Linear}(\tilde{\mathbf{G}}_m)), \quad (4)$$

$$e_i = \text{RELU}(\text{BN}(\text{Stack}(\tilde{\mathbf{E}} \odot \mathbf{E}_i))), \quad i = 1, \dots, z, \quad (5)$$

where  $\sigma$  represents the sigmoid function, which constrains the output values between 0 and 1, and  $\odot$  denotes the Hadamard product. BN stands for batch normalization, and RELU denotes the activation function. By this method, the input features  $\tilde{\mathbf{G}}_m$  are transformed into token sequences from different views, which can be further processed by subsequent layers.

Before passing to the next layers, the embedding  $\mathbf{e}$  is prepended with a learnable class token  $\mathbf{E}_{cls}$ , which serves to aggregate information from the entire sequence. To integrate positional and modality information, learnable positional embeddings  $\mathbf{E}_{pos}$  and modality embeddings  $\mathbf{E}_{mod}$  are added to the input embeddings. This approach ensures that the input

encompasses not only the sequence content but also positional and modality information:

$$\tilde{\mathbf{e}} = [\mathbf{E}_{cls}, e_1, \dots, e_z] + \mathbf{E}_{pos} + \mathbf{E}_{mod}. \quad (6)$$

The core component of the Transformer is the multi-head self-attention mechanism [41]. The embedding  $\tilde{\mathbf{e}}$  is transformed into query  $\mathbf{Q}$ , key  $\mathbf{K}$ , and value  $\mathbf{V}$  through three linear layers, with the calculation formula as follows:

$$\text{Attention}(\mathbf{Q}, \mathbf{K}, \mathbf{V}) = \text{softmax}\left(\frac{\mathbf{Q}\mathbf{K}^T}{\sqrt{d_e}}\right)\mathbf{V}, \quad (7)$$

where  $d_e$  is the dimension of the embedding. Then we use  $h$  heads for self-attention, with each head represented as  $\mathbf{H} = \text{Attention}(\mathbf{Q}, \mathbf{K}, \mathbf{V})$ . The output of the multi-head attention is  $\text{Concat}(\mathbf{H}_1, \mathbf{H}_2, \dots, \mathbf{H}_h)\mathbf{W}$ , where  $\mathbf{W}$  is the weight matrix. Subsequently, after further processing by a feed-forward neural network (FFN), then repeat twice. Incorporating emotional prompt (learnable token) [42] boosts the model's sensitivity to emotional changes. We can simply denote the entire encoder as  $f_m$ :

$$\mathbf{H}_{i,S}^m = f_m(\tilde{\mathbf{X}}_{i,S}^m). \quad (8)$$

#### 2) Long- and Short-Term Temporal Contrastive Learning:

To align the stimuli across subjects and achieve physiological synchronization among different subjects, the features extracted by the encoder are used for intra-modal temporal contrastive learning (TCL). Different values of  $t$  are used to perform contrastive learning at different time resolutions, and the corresponding encoders are pre-trained accordingly. Inspired by the SimCLR framework [32], a nonlinear projection head is employed between the encoder and the final contrastive loss. The structure, shown in Fig. 3, is used to process the features extracted by the encoder:

$$\begin{aligned} \mathbf{h}_{1,i,S}^m &= \text{ReLU}(\text{BN}(W_1\mathbf{H}_{i,S}^m + b_1)) \\ \mathbf{h}_{2,i,S}^m &= \text{Dropout}(\text{BN}(W_2\mathbf{h}_{1,i,S}^m + b_2)) \\ \mathbf{z}_{i,S}^m &= W_3\mathbf{h}_{2,i,S}^m + b_3 \end{aligned} \quad (9)$$

where  $W_1, W_2, W_3$  are the weight matrices of the three linear layers;  $b_1, b_2, b_3$  are the bias vectors and  $\mathbf{h}_{2,i,S}^m, \mathbf{h}_{1,i,S}^m, \mathbf{z}_{i,S}^m$  denote the output features of each layer. where  $i$  denotes the number of physiological signal segments,  $S$  denotes the subject. Subsequently, the similarity between samples is calculated using the following formula:

$$s(\mathbf{z}_{i,A}^m, \mathbf{z}_{j,B}^m) = \frac{\mathbf{z}_{i,A}^m \cdot \mathbf{z}_{j,B}^m}{\|\mathbf{z}_{i,A}^m\| \|\mathbf{z}_{j,B}^m\|}, \quad s(\mathbf{z}_{i,A}^m, \mathbf{z}_{j,B}^m) \in [0, 1] \quad (10)$$

Similar to the SimCLR, we use the normalized temperature-scaled cross-entropy to define the loss function as follows:

$$\begin{aligned} \mathcal{L}_{i,A}^m &= -\log\left(\frac{S_1}{S_2 + S_3}\right) \\ S_1 &= \exp\left(\frac{s(\mathbf{z}_{i,A}^m, \mathbf{z}_{i,B}^m)}{\tau}\right) \\ S_2 &= \sum_{j=1}^{5K} \mathbb{I}_{[j \neq i]} \exp\left(\frac{s(\mathbf{z}_{i,A}^m, \mathbf{z}_{j,A}^m)}{\tau}\right) \\ S_3 &= \sum_{j=1}^{5K} \exp\left(\frac{s(\mathbf{z}_{i,A}^m, \mathbf{z}_{j,B}^m)}{\tau}\right) \end{aligned} \quad (11)$$

where the indicator function  $\mathbb{I}_{[i \neq j]}$  equals 1 when  $i \neq j$ , and 0 otherwise. By minimizing this loss function, the model increases the similarity of positive pairs while reducing the



---

**Algorithm 1** The Pre-Training Procedure for PhysioSync
 

---

- 1: **Input:** Training data  $X^{eeg}$  and  $X^{pps}$
- 2: Initialize the parameters of the base encoders  $\theta^{eeg}$ ,  $\theta^{pps}$  and the projector  $\theta^{pr-eeg}$ ,  $\theta^{pr-pps}$
- 3: **for** epoch = 1 to  $T$  **do**
- 4:   **repeat**
- 5:     Sample two subjects  $A, B$ , Random scramble after segmentation  $\{X_{i,S}^m | i = 1, \dots, N; S \in \{A, B\}\}$
- 6:     Randomly select  $K$  segments  $G_m = \{X_{i,S}^m | i = 1, \dots, K; S \in \{A, B\}\}$
- 7:     Obtain  $\tilde{G}_m = \{\tilde{X}_{i,S}^m | i = 1, \dots, 5K; S \in \{A, B\}\}$  by data augmentation
- 8:     Obtain  $\{z_{i,S}^m | i = 1, \dots, 5K; S \in \{A, B\}\}$  by (3)-(9)
- 9:     Calculate loss  $L_m$  and  $L_{cc}$  by (10)-(12), then obtain total loss  $L$  by (13)
- 10:    Abate loss  $L$  through optimizer updating parameters of  $\theta^{eeg}$ ,  $\theta^{pps}$ ,  $\theta^{pr-eeg}$  and  $\theta^{pr-pps}$
- 11:   **until** all possible pairs of subjects are enumerated
- 12:   **end for**
- 13: **Output:** Parameters  $\theta^{eeg}$ ,  $\theta^{pps}$

Where  $T$  is the training epochs.

---

similarity of negative pairs. The loss for the mini-batch  $L_m$  is given by:

$$L_m = \sum_{i=1}^{5K} (\mathcal{L}_{i,A}^m + \mathcal{L}_{i,B}^m). \quad (12)$$

3) *Cross-Modal Consistency Alignment:* To align physiological signals from different modalities, the features extracted by the encoder are also used for cross-modal contrastive learning (CM-CL). Physiological signal segments from different modalities induced by the same stimulus are treated as positive pairs, while others are treated as negative pairs. Additionally, before calculating the similarity, the features pass through a linear layer to obtain  $\tilde{z}_{i,s}^m$ . Then according to formulas (10)–(12), the cross-modal contrastive loss  $L_{cc}$  is computed.

During the pre-training phase, the total loss  $L$  consists of the contrastive loss within the EEG modality  $L_{eeg}$ , the contrastive loss within peripheral physiological signals  $L_{pps}$ , and the cross-modal contrastive loss  $L_{cc}$ :

$$L = \alpha \cdot L_{eeg} + \beta \cdot L_{pps} + \gamma \cdot L_{cc}. \quad (13)$$

After pre-training, the encoder can effectively extract consistency features across different modalities at various time resolutions. Algorithm 1 summarizes the pre-training process.

### C. Supervised Fine-tuning Framework

During the pre-training stage, we obtain modality-specific encoders at different time resolutions, which are subsequently used for supervised fine-tuning in the downstream task. Specifically, the pre-trained encoders are employed to extract consistency features for EEG and PPS at long or short time resolutions (the short-term input is derived by decomposing the long-term input into 1s). Then their long-term and short-term features are fused by concatenation separately into  $H_{eeg}$  and  $H_{pps}$ , which are then input into the modal fusion module.

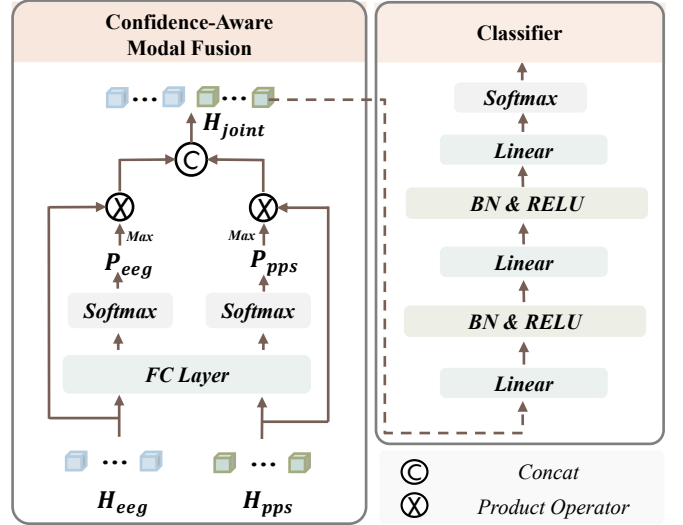


Fig. 4. The illustration of Modal Fusion Module and Classifier. In the Modal Fusion Module, we employ the Maximum Class Probability (MCP) to calculate confidence levels and assign weights to each modality accordingly.

In the Modal Fusion Module (Fig. 4), to flexibly adjust the information flow, we use Maximum Class Probability (MCP) to compute the confidence level of each modality and assign weights to the features based on their confidence. MCP enhances the robustness and accuracy of the fusion process by measuring the confidence of each modality, ensuring more reliable decision-making in the presence of uncertain or noisy data:

$$MCP(H_m) = \max_{k \in \mathbf{y}} P(Y = k | w, H_m), \quad (14)$$

where  $w$  represents the set of network parameters,  $m$  can represent both eeg or pps. Subsequently, the weighted features from both modalities are concatenated. This combined feature  $H_{joint}$  is then fed into a classifier for final classification, and we optimize the model using cross-entropy loss.

$$L_{CE} = -\mathbf{y} \log P(H_{joint}) - (1 - \mathbf{y}) \log(1 - P(H_{joint})), \quad (15)$$

where  $P(H_{joint})$  represents the probability that the joint feature vector belongs to a certain class, and  $\mathbf{y}$  denotes the sample label.

## IV. EXPERIMENTS

Our method PhysioSync is experimented and evaluated on two widely used multimodal physiological signaling datasets: the DEAP dataset containing 32 subjects and the DREAMER dataset containing 23 subjects [43], [44]. This section first describes the DEAP and DREAMER datasets in detail and the related implementation details. We then show the results of various experiments on both datasets.

### A. Dataset

1) *DEAP:* A multimodal physiological signal dataset used for emotion recognition, encompassing electroencephalogram (EEG) signals and several peripheral physiological signals. We

primarily utilized EEG, galvanic skin response (GSR), electromyography (EMG), and electrooculography (EOG). These signals were recorded from 32 subjects as they watched 40 different short videos, with each recording session lasting 63 seconds (60 seconds for emotional arousal and 3 seconds for baseline). The Self-Assessment Manikin (SAM) [45] was utilized to capture the emotional ratings of the subjects, which included assessments of arousal, valence, liking, and dominance for each video, rated on a scale from 1 to 9. In this experiment, we utilized arousal and valence as the classification criteria. When the ratings are greater than or equal to 5, they are labeled as high arousal or high valence. Conversely, ratings below 5 are labeled as low arousal or low valence. This approach forms a binary classification for each dimension, and the combination of the two dimensions results in a four-class classification.

2) *DREAMER*: The dataset comprises 14-channel EEG and 2-channel Electrocardiogram (ECG) data from 23 subjects (14 males and 9 females). Each subject viewed 18 movie clips, with durations ranging from 65 to 393 seconds. These clips were designed to elicit various emotions, including amusement, excitement, happiness, calmness, anger, disgust, fear, sadness, and surprise. Following each clip, subjects provided subjective evaluations of valence, arousal, and dominance using the Self-Assessment Manikin (SAM) on a scale from 1 to 5. The midpoint of the scale served as the threshold value: ratings of 3 or below indicated low valence or arousal, while ratings above 3 indicated high valence or arousal.

TABLE I  
SUMMARY OF THE DEAP, DREAMER DATABASES.

Databases	DEAP	DREAMER
Participants	32	23
Emotional stimuli	Musical videos	Movie clips
Trials for a participant	40	18
Physiological modalities	7	2
Target emotional classes	Binary	Binary

### B. Data Pre-processing

In the DEAP dataset, each trial lasts 63 seconds (60 seconds of emotion-inducing signals and 3 seconds of baseline). To improve accuracy, we removed the 3-second baseline by averaging it to a 1-second segment and subtracting it from the remaining 60 seconds of signals [52]. The baseline-corrected signals were then segmented into 5-second clips, resulting in 480 clips from 40 videos. With 32 participants, this gave 15,360 segments for 10-fold cross-validation. A similar baseline correction was applied to the DREAMER dataset, where each trial ranged from 65 to 395 seconds, and data was segmented into 1-second windows for pre-training and classification.

During the pre-training phase, we organized the dataset tensor along five dimensions: *video clips*, *subjects*, *1*, *channels*, and *sampling points*. In each fold, every epoch iterated through all the *video clips* in the current training data. In the fine-tuning phase, applying the same criteria, we divided the data

along the *video clips* dimension and then reshaped the first two axes—*video clips* and *subjects*—into a sample axis. After reshaping, each axis of the dataset corresponded to *samples*, *1*, *channels*, and *sampling points*.

### C. Experimental Setup

All training and experiments were conducted on an NVIDIA TITAN RTX GPU. Due to the limited number of subjects in the dataset, the results in [16], [20], [26], [53] show significant data fluctuations when evaluated with cross-subject criteria, with some standard deviations exceeding 10, affecting the reliability. Therefore, we prioritize a subject-dependent criterion. For fair comparison, all experiments followed the same procedure. We used ten-fold cross-validation, saving the best model from each fold during pre-training, which was later fine-tuned for downstream tasks. The final results were the mean and standard deviation from these folds.

With an input signal length of  $t = 1s$  for short-term and  $t = 5s$  for long-term segments, they are used to train encoders for each time scale during pre-training, with long- and short-term feature extraction performed during fine-tuning. Data augmentation included scaling the samples with factors from [0.7, 0.8] and [1.2, 1.3], and adding Gaussian noise with zero mean to ensure an SNR of 5dB. For the hyperparameters,  $\alpha$ ,  $\beta$ , and  $\gamma$  are set to 0.5, 0.5, and 1, respectively.

To optimize the contrastive learning model, we set the number of training epochs to 500, used the Adam optimizer [54], and applied a cosine annealing learning rate scheduler with triple cyclic warm restarts [55]. The initial learning rate was set to 0.0001. During fine-tuning, the emotion classification task is simpler than feature extraction. To preserve the pre-trained features and avoid overfitting on the small dataset, we set the number of epochs to 15, initial learning rate to 0.001, and batch size to 256, based on empirical observations. Other parameters remained unchanged.

### D. Performance Comparison with SOTA Models

To demonstrate the superiority of the proposed method, we conducted extensive performance comparisons on the DEAP and DREAMER datasets (see Table II and III). First, we selected several EEG-only models, including the classical SimCLR [32], a self-supervised SGMFC framework [36], a lightweight LResCapsule network [46], a CapsNet-based method [47] and DTNET [48]. Results for these "\*" models were obtained via ten-fold cross-validation using published source code and consistent experimental criteria. Additionally, we compared several multimodal fusion models. For DEAP, these include a unified cross-attention method called TACOformer [49], a dynamic confidence-aware fusion network (CAFNet) [16], a multimodal long short-term memory network (MFST-RNN) [50], and an Incongruity-aware multimodal physiology signal fusion network (IANet) [31]. For DREAMER, we included TACOformer [49] and DCCA [51].

As shown in Tables II and III, our proposed method outperforms all others. Specifically, for the arousal, valence, and four-class classification tasks, the average recognition accuracies are 98.35%, 98.17%, and 97.99% for DEAP, and

TABLE II

PERFORMANCE COMPARISON WITH SOAT SCHEMES IN TERMS OF ACCURACY (%) AND F1 SCORE (%) ON THE DEAP DATASET. WHERE \* INDICATES THAT THE RESULTS OF THIS MODEL WERE REPRODUCED BY OURSELVES, WHILE THE OTHERS ARE RESULTS REPORTED IN THE PAPER.

Method	Modalities	Arousal		Valence		Four	
		ACC $\pm$ Std (%)	F1 $\pm$ Std (%)	ACC $\pm$ Std (%)	F1 $\pm$ Std (%)	ACC $\pm$ Std (%)	F1 $\pm$ Std (%)
SimCLR* [32]	EEG	92.25 $\pm$ 0.63	93.43 $\pm$ 0.56	91.39 $\pm$ 0.58	92.38 $\pm$ 0.68	90.83 $\pm$ 0.91	90.82 $\pm$ 0.92
SGMC* [36]	EEG	95.01 $\pm$ 0.45	95.87 $\pm$ 0.42	94.56 $\pm$ 0.39	94.91 $\pm$ 0.37	92.32 $\pm$ 0.47	92.35 $\pm$ 0.45
LResCapsule* [46]	EEG	96.16 $\pm$ 0.38	96.98 $\pm$ 0.41	95.87 $\pm$ 0.35	96.53 $\pm$ 0.32	93.96 $\pm$ 0.36	93.95 $\pm$ 0.31
CapsNet* [47]	EEG	96.70 $\pm$ 1.01	97.93 $\pm$ 1.03	97.10 $\pm$ 1.23	98.04 $\pm$ 1.11	96.98 $\pm$ 1.17	97.16 $\pm$ 1.09
DTNET [48]	EEG	98.17 $\pm$ 1.06	—	98.13 $\pm$ 1.12	—	—	—
TACOformer [49]	EEG, PPS	92.02 $\pm$ 0.73	—	91.59 $\pm$ 0.51	—	—	—
MFST-RNN [50]	EEG, PPS	95.89 $\pm$ 1.72	96.09 $\pm$ —	94.99 $\pm$ 1.73	95.30 $\pm$ —	—	—
CAFNet [16]	EEG, Facial	94.89 $\pm$ 3.07	95.55 $\pm$ 3.30	95.25 $\pm$ 3.84	94.50 $\pm$ 3.97	—	—
IANet [31]	EEG, EOG, EMG, GSR	97.56 $\pm$ 2.64	97.55 $\pm$ 2.64	97.42 $\pm$ 1.93	97.41 $\pm$ 1.94	—	—
Ours	EEG, GSR	<b>98.35 <math>\pm</math> 0.41</b>	<b>98.61 <math>\pm</math> 0.32</b>	<b>98.17 <math>\pm</math> 0.59</b>	<b>98.40 <math>\pm</math> 0.52</b>	<b>97.99 <math>\pm</math> 0.49</b>	<b>97.99 <math>\pm</math> 0.48</b>

TABLE III

PERFORMANCE COMPARISON WITH SOAT SCHEMES IN TERMS OF ACCURACY (%) AND F1 SCORE (%) ON THE DREAMER DATASET.

Method	Modalities	Arousal		Valence		Four	
		ACC $\pm$ Std (%)	F1 $\pm$ Std (%)	ACC $\pm$ Std (%)	F1 $\pm$ Std (%)	ACC $\pm$ Std (%)	F1 $\pm$ Std (%)
SimCLR* [32]	EEG	91.36 $\pm$ 0.71	92.68 $\pm$ 0.64	91.11 $\pm$ 0.68	92.32 $\pm$ 0.59	90.17 $\pm$ 0.37	90.15 $\pm$ 0.38
SGMC* [36]	EEG	95.35 $\pm$ 0.35	96.28 $\pm$ 0.38	94.25 $\pm$ 0.37	95.12 $\pm$ 0.33	90.28 $\pm$ 0.28	91.26 $\pm$ 0.35
LResCapsule* [46]	EEG	96.39 $\pm$ 0.22	96.76 $\pm$ 0.26	94.57 $\pm$ 0.29	95.13 $\pm$ 0.25	92.94 $\pm$ 0.29	92.88 $\pm$ 0.31
CapsNet* [47]	EEG	96.02 $\pm$ 0.90	95.98 $\pm$ 0.91	95.01 $\pm$ 0.88	95.48 $\pm$ 0.90	93.31 $\pm$ 0.94	93.46 $\pm$ 0.98
DTNET [48]	EEG	95.17 $\pm$ 4.78	—	95.62 $\pm$ 4.46	—	—	—
DCCA [51]	EEG, ECG	89.00 $\pm$ 2.80	—	90.60 $\pm$ 4.10	—	—	—
TACOformer [49]	EEG, ECG	94.03 $\pm$ 1.71	—	94.58 $\pm$ 4.73	—	—	—
Ours	EEG, ECG	<b>97.01 <math>\pm</math> 0.31</b>	<b>97.55 <math>\pm</math> 0.38</b>	<b>96.11 <math>\pm</math> 0.32</b>	<b>96.89 <math>\pm</math> 0.25</b>	<b>94.70 <math>\pm</math> 0.25</b>	<b>94.69 <math>\pm</math> 0.25</b>

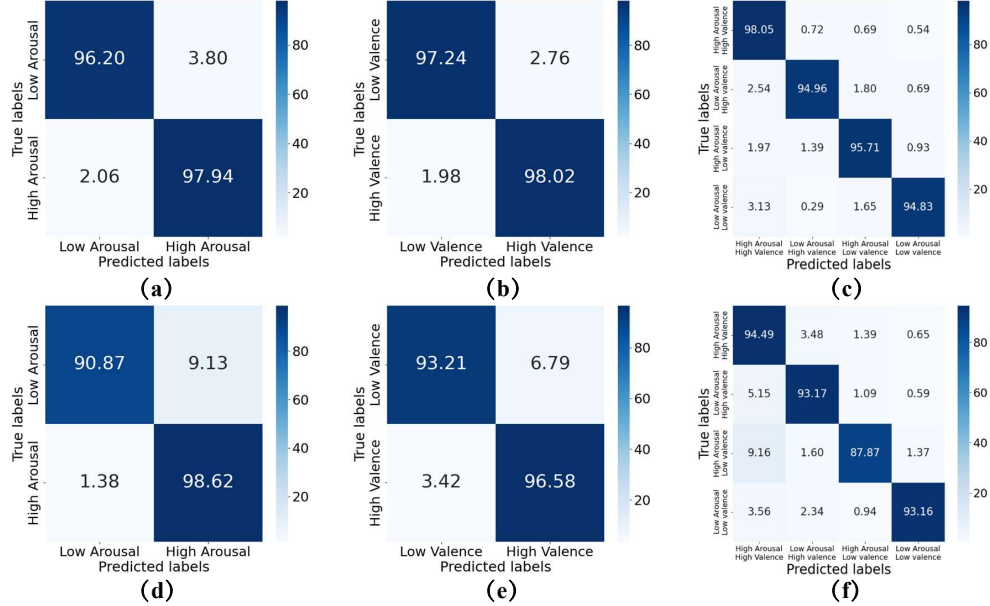


Fig. 5. Confusion matrices in the DEAP and DREAMER datasets. (a) DEAP-Arousal. (b) DEAP-Valence. (c) DEAP-Four. (d) DREAMER-Arousal. (e) DREAMER-Valence. (f) DREAMER-Four.

97.01%, 96.11%, and 94.70% for DREAMER. The corresponding F1 scores are 98.61%, 98.40%, and 97.99% for DEAP, and 97.55%, 96.89%, and 94.69% for DREAMER. Compared to models using EEG alone, our method achieves a recognition accuracy increase of 1.65% in arousal, 1.07% in valence, and 1.31% in the four-class on the DEAP dataset. In the DREAMER dataset, the accuracy increases by 0.62% in arousal, 1.10% in valence, and 1.39% in the four-class, indicating that the two modalities complement each other,

providing more comprehensive emotional information.

Similarly, compared to other multimodal models, our method improves recognition accuracy by 0.79% in arousal and 0.75% in valence on the DEAP dataset, and by 2.98% in arousal and 1.53% in valence on the DREAMER dataset. This demonstrates that our model more effectively leverages multimodal physiological information, reducing both heterogeneity and redundancy. Similarly, the F1 score also shows varying degrees of improvement. Moreover, both the accuracy

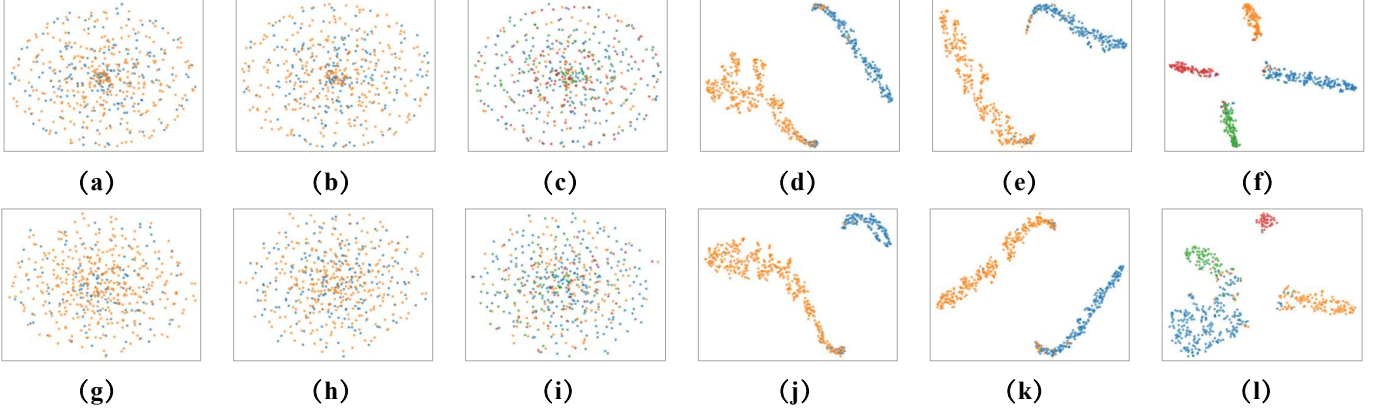


Fig. 6. T-SNE visualization in the DEAP and DREAMER datasets. The original feature distributions of arousal, valence, and the four-class for the DEAP and DREAMER datasets are represented by (a)-(c) and (g)-(i), respectively. The feature distributions of our method across various dimensional spaces for both datasets are shown in (d)-(f) and (j)-(l). In the two-color image,  $\bullet$  represent the low and high arousal (or valence), respectively. In the four-color image,  $\bullet$  represent high arousal/high valence, low arousal/high valence, high arousal/low valence and low arousal/low valence, respectively.

TABLE IV  
ABLATION EXPERIMENTS ON THE DEAP DATASET. TCL REPRESENTS INTRA-MODAL TEMPORAL CONTRASTIVE LEARNING, DA REPRESENTS DATA AUGMENTATION, CM-CL REPRESENTS CROSS-MODAL CONTRASTIVE LEARNING.

Method	TCL	DA	CM-CL	Arousal		Valence		Four	
				ACC $\pm$ Std (%)	F1 $\pm$ Std (%)	ACC $\pm$ Std (%)	F1 $\pm$ Std (%)	ACC $\pm$ Std (%)	F1 $\pm$ Std (%)
Ours-1				95.96 $\pm$ 0.71	97.01 $\pm$ 0.73	95.91 $\pm$ 0.60	96.90 $\pm$ 0.78	95.32 $\pm$ 0.51	95.31 $\pm$ 0.50
Ours-2	✓			96.99 $\pm$ 0.51	97.23 $\pm$ 0.49	97.03 $\pm$ 0.56	97.58 $\pm$ 0.51	96.15 $\pm$ 0.63	96.10 $\pm$ 0.75
Ours-3	✓	✓		97.35 $\pm$ 0.46	97.63 $\pm$ 0.48	97.16 $\pm$ 0.41	97.56 $\pm$ 0.43	96.92 $\pm$ 0.43	96.93 $\pm$ 0.44
Ours	✓	✓	✓	<b>97.92 <math>\pm</math> 0.51</b>	<b>98.25 <math>\pm</math> 0.38</b>	<b>98.01 <math>\pm</math> 0.42</b>	<b>98.22 <math>\pm</math> 0.38</b>	<b>97.65 <math>\pm</math> 0.32</b>	<b>97.66 <math>\pm</math> 0.31</b>

and F1 scores have a standard deviation (STD) not exceeding 0.6. In summary, our approach not only enhances performance but also improves the reliability and stability of emotion recognition using multimodal physiological signals.

### E. Qualitative Analysis

In this section, we provide a detailed visual analysis to investigate the challenges associated with emotion recognition. Fig. 5 displays the confusion matrices of the proposed model on the DEAP and DREAMER datasets, highlighting its ability to distinguish various emotional states. In both datasets, high values in the arousal and valence dimensions correspond to higher accuracy, with high valence and high arousal typically linked to discrete emotions such as happiness, excitement, and pleasure. These positive emotions are often associated with distinct physiological patterns, including increased heart rate, skin conductance, and brain activity, making them easier to recognize. Further, when arousal and valence are combined into four categories, the best performance is observed in the high valence/high arousal category for both datasets, which is consistent with the conclusion from the previous binary classification.

To further illustrate the classification capabilities of the model, we utilized t-SNE for dimensionality reduction to visually compare the distribution of raw features and the feature distribution after model training (see Fig. 6). In the trained feature distribution, the separation between emotion categories is significantly improved, where features from different categories exhibit clear clustering trends across all

dimensions. This result indicates a significant advancement in the model’s feature extraction and emotion classification performance, enabling it to more effectively identify and distinguish latent patterns in emotional data. Additionally, the trained features exhibit a continuous band-like distribution, highlighting the smoothness of emotion labels. This suggests that emotion recognition relies not only on instantaneous emotional changes but also on the dynamic and time-dependent nature of emotions.

## V. ABLATION EXPERIMENTS

This section presents a series of ablation experiments. Notably, to control for confounding factors, all experiments during fine-tuning utilized only long-term features, except for the ablation experiment of the long short term strategy.

### A. Analysis of Data Augmentation and Contrastive Learning

To validate the effectiveness of each module, we conducted multiple ablation experiments by sequentially adding each module (see Table IV). Three components were selected for ablation studies: intra-modal temporal contrastive learning (TCL), data augmentation (DA), and cross-modal contrastive learning (CM-CL). By applying intra-modal temporal contrastive learning, the corresponding encoders are able to extract physiological signal features that are consistent with the stimuli, making it easier to distinguish different emotional states in downstream classification tasks and achieve physiological synchronization across subjects. Data augmentation increases the amount of trainable data while introducing more positive



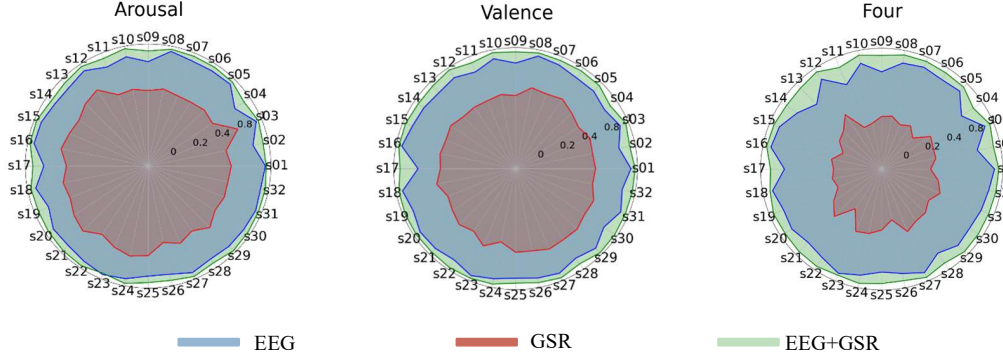


Fig. 7. The recognition accuracy of arousal, valence, and four dimensions of each subject in DEAP dataset by using EEG, GSR, and modality fusion.

pairs, providing additional samples for contrastive learning and enhancing the model’s generalization ability. Cross-modal contrastive learning strengthens the interaction and alignment effects between modalities, aligning signals from different modalities in a shared semantic space, thereby achieving physiological synchronization across physiological signals. The results show that as the modules are added, the recognition performance steadily increases, confirming the effectiveness of each component in our proposed method.

### B. Ablation of EEG and PPS

To validate the complementary role of PPS to EEG, we conducted a modality ablation experiment on the DEAP dataset. We tested four modalities—EEG, Electromyography (EMG), Electrooculography (EOG), and GSR—both individually and in combination, as summarized in Table see Figure V. The results show that incorporating peripheral physiological signals improved recognition accuracy by 2.91% in arousal and 3.03% in valence, while F1 scores increased by 1.47% in arousal and 1.66% in valence. Specifically, the combination of EEG and GSR yielded the best results across most dimensions. The SOTA comparison experiment results are based on the fusion of EEG and GSR. Among the single modalities, EEG consistently achieved the highest accuracy and F1 scores across the Arousal, Valence, and four-category tasks, further emphasizing its critical role in emotion recognition.

TABLE V  
COMPARISON OF THE PERFORMANCE OF SINGLE MODALITY AND PAIRWISE DIFFERENT MODALITY COMBINATIONS.

Modality	Arousal		Valence	
	ACC $\pm$ Std (%)	F1 $\pm$ Std (%)	ACC $\pm$ Std (%)	F1 $\pm$ Std (%)
EEG	95.01 $\pm$ 0.47	96.78 $\pm$ 0.45	94.98 $\pm$ 0.28	96.56 $\pm$ 0.44
EMG	59.93 $\pm$ 1.20	62.30 $\pm$ 1.98	60.15 $\pm$ 1.45	63.91 $\pm$ 1.68
EOG	64.70 $\pm$ 1.83	68.56 $\pm$ 1.89	62.05 $\pm$ 1.95	67.86 $\pm$ 2.11
GSR	63.19 $\pm$ 2.29	66.76 $\pm$ 2.86	63.09 $\pm$ 2.35	65.53 $\pm$ 2.18
EEG + GSR	<b>97.92 <math>\pm</math> 0.51</b>	<b>98.25 <math>\pm</math> 0.38</b>	<b>98.01 <math>\pm</math> 0.42</b>	<b>98.22 <math>\pm</math> 0.38</b>
EEG + EMG	97.73 $\pm$ 0.54	98.08 $\pm$ 0.48	97.77 $\pm$ 0.59	98.03 $\pm$ 0.55
EEG + EOG	97.85 $\pm$ 0.46	98.19 $\pm$ 0.39	97.55 $\pm$ 0.59	97.82 $\pm$ 0.60

We further conducted experiments using the EEG and GSR data from each subject separately to validate the role of modality fusion. As shown in Fig. 7, the fusion of EEG and GSR (green line) consistently outperformed the single modalities (EEG in blue and GSR in red) across all 32 subjects

in the arousal, valence, and four-class classification tasks. This demonstrates the complementary nature of EEG and GSR, highlighting the strength of modality fusion in providing a richer and more robust representation of emotional states.

### C. Ablation of Long-Term Signal Decomposition for Short-Term Fusion

In the final fine-tuning strategy, we combined long-term and short-term temporal features. Here, “Long” refers to using only long-term features, “Long+Short” uses a fusion of both long- and short-term features, and “Long\*” adds two self-attention layers on top of the “Long” strategy. Specifically (see Table VI), compared to using long-term features alone, further fusion with short-term features improves recognition accuracy by 0.43% in arousal and 0.16% in valence, and F1 scores increased by 0.43% in arousal and 0.18% in valence. The performance improvement highlights the value of multi-scale feature integration in emotion recognition. In contrast, adding parameters with the “Long\*” strategy alone does not improve performance, indicating that relying solely on long-term features, even with more parameters, limits the model’s capacity to capture dynamic emotional changes.

TABLE VI  
COMPARISON OF CLASSIFICATION RESULTS FOR LONG-TIME FEATURES AND FUSION OF LONG-SHORT TIME FEATURES.

Method	Params	Arousal		Valence	
		ACC $\pm$ Std (%)	F1 $\pm$ Std (%)	ACC $\pm$ Std (%)	F1 $\pm$ Std (%)
Long	116M	97.92 $\pm$ 0.51	98.25 $\pm$ 0.38	98.01 $\pm$ 0.42	98.22 $\pm$ 0.38
Long*	141M	97.35 $\pm$ 0.45	97.86 $\pm$ 0.54	97.21 $\pm$ 0.47	97.74 $\pm$ 0.46
Long + Short	142M	<b>98.35 <math>\pm</math> 0.41</b>	<b>98.61 <math>\pm</math> 0.32</b>	<b>98.17 <math>\pm</math> 0.59</b>	<b>98.40 <math>\pm</math> 0.52</b>

### D. Impact of Various Time Resolutions (Windows)

In this section, we systematically examine the effect of time window length on model performance in emotion recognition using physiological signals (see Fig. 8). We evaluated signal segments of varying durations (1 to 10 seconds, excluding 7s, 8s, and 9s). The results show a clear trend: classification performance improves significantly as the time window length increases, especially between 1 and 6 seconds. This is reflected in both accuracy and F1 scores, suggesting that longer signal segments capture richer physiological features.

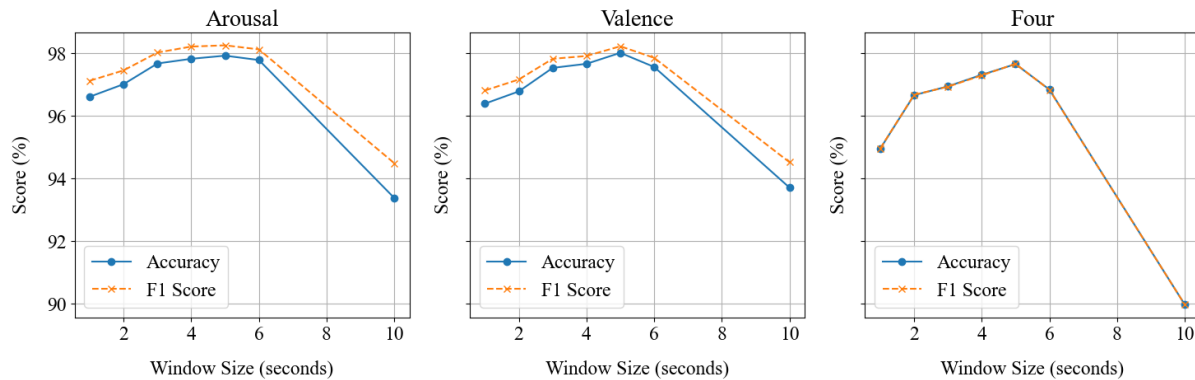


Fig. 8. Illustration of model performance with different time windows on the DEAP dataset. The best performance is achieved with a 5-second window.

Performance peaks at 5 seconds, offering the best balance between accuracy and computational efficiency. Beyond this, longer windows lead to a performance decline, likely due to noise or redundancy. Overall, a 5-second window strikes the optimal trade-off between performance and efficiency.

#### E. Comparison of Physiological Signal Pairing Strategies

To validate the effectiveness of our positive-negative pair selection strategy, we compared it with CLISA [20], the best-performing single-modality method using only EEG. In CLISA, 5-second segments are randomly selected from each trial and paired across subjects as positive pairs. Our method pre-divides each trial into chronological 5-second segments, randomly selects  $K$  segments, and generates negative pairs within the same trial. This increases the challenge of contrastive learning through more refined sample pairing. As shown in Table VII (Our\* means that our method does not use data augmentation), our construction method better helps the model distinguish between different emotional categories. Specifically, accuracy and F1 scores improved by 0.34% and 1.54% in arousal, 0.38% and 1.35% in valence, while corresponding standard deviations decreased by  $0.06 \sim 0.41$  and  $0.21 \sim 0.37$ , respectively. Our intra-trial negative pairing surpasses CLISA by learning fine-grained within-subject emotional differences, boosting robustness and discriminability.

TABLE VII  
PERFORMANCE OF SELECTION STRATEGIES USING DIFFERENT POSITIVE AND NEGATIVE PAIRS.

Method	Arousal		Valence	
	ACC $\pm$ Std (%)	F1 $\pm$ Std (%)	ACC $\pm$ Std (%)	F1 $\pm$ Std (%)
CLISA [20]	94.67 $\pm$ 0.53	95.26 $\pm$ 0.67	94.60 $\pm$ 0.72	95.21 $\pm$ 0.81
Ours*	94.81 $\pm$ 0.51	95.35 $\pm$ 0.59	94.55 $\pm$ 0.39	95.85 $\pm$ 0.62
Ours	<b>95.01 <math>\pm</math> 0.47</b>	<b>96.78 <math>\pm</math> 0.45</b>	<b>94.98 <math>\pm</math> 0.41</b>	<b>96.56 <math>\pm</math> 0.44</b>

#### F. Ablation of Modal Fusion Strategies

In downstream tasks involving the fusion of different modalities, we compared several common fusion methods, including feature-level fusion [56], decision-level fusion [57], adaptive weighting [58], attention mechanisms [59], and cross-attention

[60] (see Fig. 9). The decision-level fusion combines the final outputs of the classification head, while other methods perform fusion on the features extracted by the encoder. The results show that our fusion method outperforms others in terms of performance. By assigning a weight to each modality based on its maximum class probability before fusion, our method ensures an appropriate contribution from each modality, enabling the model to prioritize the most informative signals while still considering all modalities.

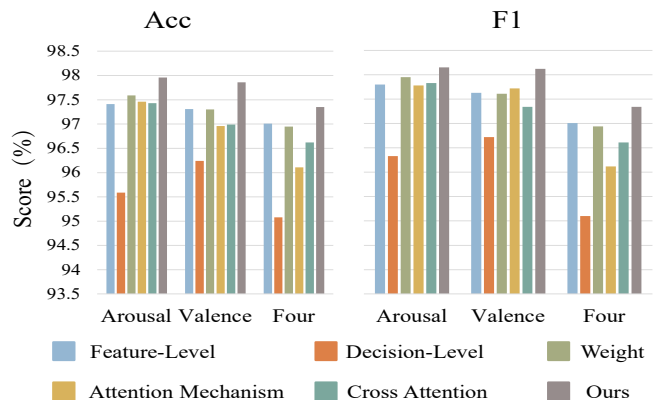


Fig. 9. Comparison of different modal fusion methods (Including feature-level fusion, decision-level fusion, adaptive weighting, attention mechanisms, and cross-attention).

## VI. LIMITATION

In this study, we chose a subject-dependent experimental criteria due to large fluctuations observed in cross-subject results, with standard deviations exceeding 10 in some cases. A similar trend was found in other studies using cross-subject criteria [16], [20], [26], [53], which may be largely attributed to the limited number of subjects involved in the dataset. Therefore, we ultimately adopted a subject-dependent criteria. This experimental setup yields stable results, with standard deviations not exceeding 1, ensuring the reliability of the outcomes. To ensure a fair comparison, we reproduced several baseline methods using open-source code, making sure that comparisons were conducted under the same experimental

conditions. For methods that could not be reproduced, we selected those with similar experimental settings. While cross-subject experiments were not the focus of this study, they represent a valuable direction for future work, with the potential to further ensure more reliable analysis, comparison, and reporting.

## VII. CONCLUSION

In this paper, inspired by physiological synchronization, we propose a contrastive learning framework for emotion recognition, achieving competitive results on the DEAP and DREAMER datasets. By integrating intra-modal temporal contrastive learning (TCL) and cross-modal contrastive learning (CM-CL), we make preliminary attempts at achieving physiological synchronization across both subjects and modalities. Additionally, we found that a 5-second time window performed optimally when using a single time resolution feature. However, as emotions are characterized by both instantaneous and subtle changes, further extraction and fusion of long-term and short-term features from different time resolutions have led to even better results. Experiments show that, although EEG signals generally perform well in emotion recognition, a reasonable and effective combination with peripheral physiological signals can lead to even better results. Physiological signals are typically multi-channel, with spatial relationships between channels that our model has not yet fully exploited. Therefore, in addition to improving the cross-subject experiments, future research will focus on better exploring and utilizing these spatial relationships to further enhance model performance.

## REFERENCES

- [1] Xiaowei Zhang, Zhongyi Zhou, Qiqi Zhao, Kechen Hou, Xiangyu Wei, Sipo Zhang, Yikun Yang, and Yanmeng Cui. Discriminative joint knowledge transfer with online updating mechanism for eeg-based emotion recognition. *IEEE Transactions on Computational Social Systems*, 11(2):2918–2929, 2023.
- [2] Mahboobeh Jafari, Afshin Shoeibi, Marjane Khodatars, Sara Bagherzadeh, Ahmad Shalbaf, David López García, Juan M Gorriz, and U Rajendra Acharya. Emotion recognition in eeg signals using deep learning methods: A review. *Computers in Biology and Medicine*, 165:107450, 2023.
- [3] Wei-Bang Jiang, Xuan-Hao Liu, Wei-Long Zheng, and Bao-Liang Lu. Multimodal adaptive emotion transformer with flexible modality inputs on a novel dataset with continuous labels. In *Proceedings of the 31st ACM International Conference on Multimedia*, pages 5975–5984, 2023.
- [4] Soraia M Alarcão and Manuel J Fonseca. Emotions recognition using eeg signals: A survey. *IEEE transactions on affective computing*, 10(3):374–393, 2017.
- [5] Iris B Mauss and Michael D Robinson. Measures of emotion: A review. *Cognition and emotion*, 23(2):209–237, 2009.
- [6] Rui Li, Chao Ren, Chen Li, Nan Zhao, Dawei Lu, and Xiaowei Zhang. Sstd: a novel spatio-temporal demographic network for eeg-based emotion recognition. *IEEE Transactions on Computational Social Systems*, 10(1):376–387, 2022.
- [7] Ashima Khosla, Padmavati Khandnor, and Trilok Chand. A comparative analysis of signal processing and classification methods for different applications based on eeg signals. *Biocybernetics and Biomedical Engineering*, 40(2):649–690, 2020.
- [8] Xiaojun Li, CL Philip Chen, Bianna Chen, and Tong Zhang. Gusa: Graph-based unsupervised subdomain adaptation for cross-subject eeg emotion recognition. *IEEE Transactions on Affective Computing*, 2024.
- [9] Fang Liu, Pei Yang, Yezhi Shu, Niqi Liu, Jenny Sheng, Junwen Luo, Xiaolan Wang, and Yong-Jin Liu. Emotion recognition from few-channel eeg signals by integrating deep feature aggregation and transfer learning. *IEEE Transactions on Affective Computing*, 2023.
- [10] Rushuang Zhou, Zhiguo Zhang, Hong Fu, Li Zhang, Linling Li, Gan Huang, Fali Li, Xin Yang, Yining Dong, Yuan-Ting Zhang, et al. Pr-pl: A novel prototypical representation based pairwise learning framework for emotion recognition using eeg signals. *IEEE Transactions on Affective Computing*, 15(2):657–670, 2023.
- [11] Mengqing Ye, CL Philip Chen, Wenming Zheng, and Tong Zhang. Adaptive dual-space network with multigraph fusion for eeg-based emotion recognition. *IEEE Transactions on Computational Social Systems*, 2024.
- [12] Xiaoqing Gu, Weiwei Cai, Ming Gao, Yizhang Jiang, Xin Ning, and Pengjiang Qian. Multi-source domain transfer discriminative dictionary learning modeling for electroencephalogram-based emotion recognition. *IEEE Transactions on Computational Social Systems*, 9(6):1604–1612, 2022.
- [13] Jiehao Tang, Zhuang Ma, Kaiyu Gan, Jianhua Zhang, and Zhong Yin. Hierarchical multimodal-fusion of physiological signals for emotion recognition with scenario adaption and contrastive alignment. *Information Fusion*, 103:102129, 2024.
- [14] Shun Katada, Shogo Okada, and Kazunori Komatani. Effects of physiological signals in different types of multimodal sentiment estimation. *IEEE Transactions on Affective Computing*, 14(3):2443–2457, 2022.
- [15] Jian Shen, Kexin Zhu, Huakang Liu, Jinwen Wu, Kang Wang, and Qunxi Dong. Tensor correlation fusion for multimodal physiological signal emotion recognition. *IEEE Transactions on Computational Social Systems*, 2024.
- [16] Qi Zhu, Chuhan Zheng, Zheng Zhang, Wei Shao, and Daoqiang Zhang. Dynamic confidence-aware multi-modal emotion recognition. *IEEE Transactions on Affective Computing*, 2023.
- [17] Baole Fu, Wenhao Chu, Chunrui Gu, and Yinhua Liu. Cross-modal guiding neural network for multimodal emotion recognition from eeg and eye movement signals. *IEEE Journal of Biomedical and Health Informatics*, 2024.
- [18] Manju Priya Arthanarisamy Ramaswamy and Suja Palaniswamy. Subject independent emotion recognition using eeg and physiological signals—a comparative study. *Applied Computing and Informatics*, 2022.
- [19] Junnan Li, Ramprasaath Selvaraju, Akhilesh Gotmare, Shafiq Joty, Caiming Xiong, and Steven Chu Hong Hoi. Align before fuse: Vision and language representation learning with momentum distillation. *Advances in neural information processing systems*, 34:9694–9705, 2021.
- [20] Xinke Shen, Xianggen Liu, Xin Hu, Dan Zhang, and Sen Song. Contrastive learning of subject-invariant eeg representations for cross-subject emotion recognition. *IEEE Transactions on Affective Computing*, 14(3):2496–2511, 2022.
- [21] Marlies Houben, Wim Van Den Noortgate, and Peter Kuppens. The relation between short-term emotion dynamics and psychological well-being: A meta-analysis. *Psychological bulletin*, 141(4):901, 2015.
- [22] Huan Liu, Tianyu Lou, Yuzhe Zhang, Yixiao Wu, Yang Xiao, Christian S Jensen, and Dalin Zhang. Eeg-based multimodal emotion recognition: a machine learning perspective. *IEEE Transactions on Instrumentation and Measurement*, 2024.
- [23] Shuaiqi Liu, Zeyao Wang, Yanling An, Bing Li, Xinrui Wang, and Yudong Zhang. Da-capsnet: A multi-branch capsule network based on adversarial domain adaption for cross-subject eeg emotion recognition. *Knowledge-Based Systems*, 283:111137, 2024.
- [24] Xiaobing Du, Cuixia Ma, Guanhua Zhang, Jinyao Li, Yu-Kun Lai, Guozhen Zhao, Xiaoming Deng, Yong-Jin Liu, and Hongan Wang. An efficient lstm network for emotion recognition from multichannel eeg signals. *IEEE Transactions on Affective Computing*, 13(3):1528–1540, 2020.
- [25] Yongqiang Yin, Xiangwei Zheng, Bin Hu, Yuang Zhang, and Xinchun Cui. Eeg emotion recognition using fusion model of graph convolutional neural networks and lstm. *Applied Soft Computing*, 100:106954, 2021.
- [26] Yi Ding, Neethu Robinson, Su Zhang, Qiuhao Zeng, and Cuntai Guan. Tsception: Capturing temporal dynamics and spatial asymmetry from eeg for emotion recognition. *IEEE Transactions on Affective Computing*, 14(3):2238–2250, 2022.
- [27] Zhipeng He, Zina Li, Fuzhou Yang, Lei Wang, Jingcong Li, Chengju Zhou, and Jiahui Pan. Advances in multimodal emotion recognition based on brain–computer interfaces. *Brain sciences*, 10(10):687, 2020.
- [28] Youngchul Kwak, Woo-Jin Song, and Seong-Eun Kim. Fganet: fnirs-guided attention network for hybrid eeg-fnirs brain-computer interfaces. *IEEE Transactions on Neural Systems and Rehabilitation Engineering*, 30:329–339, 2022.
- [29] M Sami Zitouni, Cheul Young Park, Uichin Lee, Leontios J Hadjileontiadis, and Ahsan Khandoker. Lstm-modeling of emotion recognition using peripheral physiological signals in naturalistic conversations. *IEEE Journal of Biomedical and Health Informatics*, 27(2):912–923, 2022.

- [30] Magdiel Jiménez-Guarneros, Gibran Fuentes-Pineda, and Jonas Grande-Barreto. Mmda: A multimodal and multisource domain adaptation method for cross-subject emotion recognition from eeg and eye movement signals. *IEEE Transactions on Computational Social Systems*, 2024.
- [31] Jing Li, Ning Chen, Hongqing Zhu, Guangqiang Li, Zhangyong Xu, and Dingxin Chen. Incongruity-aware multimodal physiology signals fusion for emotion recognition. *Information Fusion*, 105:102220, 2024.
- [32] Ting Chen, Simon Kornblith, Mohammad Norouzi, and Geoffrey Hinton. A simple framework for contrastive learning of visual representations. In *International conference on machine learning*, pages 1597–1607. PMLR, 2020.
- [33] Yanru Qu, Dinghan Shen, Yelong Shen, Sandra Sajeev, Jiawei Han, and Weizhu Chen. Coda: Contrast-enhanced and diversity-promoting data augmentation for natural language understanding. *arXiv preprint arXiv:2010.08670*, 2020.
- [34] Yang Li, Guanyu Qiao, Xin Gao, and Guohua Wang. Supervised graph co-contrastive learning for drug–target interaction prediction. *Bioinformatics*, 38(10):2847–2854, 2022.
- [35] Ziyu Liu, Azadeh Alavi, Minyi Li, and Xiang Zhang. Self-supervised contrastive learning for medical time series: A systematic review. *Sensors*, 23(9):4221, 2023.
- [36] Haoning Kan, Jiale Yu, Jiajin Huang, Zihe Liu, Heqian Wang, and Haiyan Zhou. Self-supervised group meiosis contrastive learning for eeg-based emotion recognition. *Applied Intelligence*, 53(22):27207–27225, 2023.
- [37] Qile Liu, Zhihao Zhou, Jiyuan Wang, and Zhen Liang. Joint contrastive learning with feature alignment for cross-corpus eeg-based emotion recognition. *arXiv preprint arXiv:2404.09559*, 2024.
- [38] Khushboo Singh, Mitul Kumar Ahirwal, and Manish Pandey. Subject wise data augmentation based on balancing factor for quaternary emotion recognition through hybrid deep learning model. *Biomedical Signal Processing and Control*, 86:105075, 2023.
- [39] Eleonora Lopez, Eleonora Chiarantano, Eleonora Grassucci, and Danilo Comminiello. Hypercomplex multimodal emotion recognition from eeg and peripheral physiological signals. In *2023 IEEE International Conference on Acoustics, Speech, and Signal Processing Workshops (ICASSPW)*, pages 1–5. IEEE, 2023.
- [40] Guillermo Iglesias, Edgar Talavera, Ángel González-Prieto, Alberto Mozo, and Sandra Gómez-Canaval. Data augmentation techniques in time series domain: a survey and taxonomy. *Neural Computing and Applications*, 35(14):10123–10145, 2023.
- [41] A Vaswani. Attention is all you need. *Advances in Neural Information Processing Systems*, 2017.
- [42] Timothée Darcet, Maxime Oquab, Julien Mairal, and Piotr Bojanowski. Vision transformers need registers. *arXiv preprint arXiv:2309.16588*, 2023.
- [43] Sander Koelstra, Christian Muhl, Mohammad Soleymani, Jong-Seok Lee, Ashkan Yazdani, Touradj Ebrahimi, Thierry Pun, Anton Nijholt, and Ioannis Patras. Deap: A database for emotion analysis; using physiological signals. *IEEE transactions on affective computing*, 3(1):18–31, 2011.
- [44] Stamos Katsigiannis and Naeem Ramzan. Dreamer: A database for emotion recognition through eeg and ecg signals from wireless low-cost off-the-shelf devices. *IEEE journal of biomedical and health informatics*, 22(1):98–107, 2017.
- [45] Margaret M Bradley and Peter J Lang. Measuring emotion: the self-assessment manikin and the semantic differential. *Journal of behavior therapy and experimental psychiatry*, 25(1):49–59, 1994.
- [46] Cunhang Fan, Jinqin Wang, Wei Huang, Xiaoke Yang, Guangxiong Pei, Taihao Li, and Zhao Lv. Light-weight residual convolution-based capsule network for eeg emotion recognition. *Advanced Engineering Informatics*, 61:102522, 2024.
- [47] Chang Li, Bin Wang, Silin Zhang, Yu Liu, Rencheng Song, Juan Cheng, and Xun Chen. Emotion recognition from eeg based on multi-task learning with capsule network and attention mechanism. *Computers in biology and medicine*, 143:105303, 2022.
- [48] Weitong Sun and Yuping Su. Emotion recognition of eeg based on dual-input multi-network fusion features. In *2024 7th International Conference on Information Communication and Signal Processing (ICICSP)*, pages 809–817. IEEE, 2024.
- [49] Xinda Li. Tacoforner: Token-channel compounded cross attention for multimodal emotion recognition. *arXiv preprint arXiv:2306.13592*, 2023.
- [50] Qi Li, Yunqing Liu, Fei Yan, Qiong Zhang, and Cong Liu. Emotion recognition based on multiple physiological signals. *Biomedical Signal Processing and Control*, 85:104989, 2023.
- [51] Wei Liu, Jie-Lin Qiu, Wei-Long Zheng, and Bao-Liang Lu. Comparing recognition performance and robustness of multimodal deep learning models for multimodal emotion recognition. *IEEE Transactions on Cognitive and Developmental Systems*, 14(2):715–729, 2021.
- [52] Yilong Yang, Qingfeng Wu, Ming Qiu, Yingdong Wang, and Xiaowei Chen. Emotion recognition from multi-channel eeg through parallel convolutional recurrent neural network. In *2018 international joint conference on neural networks (IJCNN)*, pages 1–7. IEEE, 2018.
- [53] Weishan Ye, Zhiguo Zhang, Fei Teng, Min Zhang, Jianhong Wang, Dong Ni, Fali Li, Peng Xu, and Zhen Liang. Semi-supervised dual-stream self-attentive adversarial graph contrastive learning for cross-subject eeg-based emotion recognition. *IEEE Transactions on Affective Computing*, 2024.
- [54] Diederik P Kingma. Adam: A method for stochastic optimization. *arXiv preprint arXiv:1412.6980*, 2014.
- [55] Ilya Loshchilov and Frank Hutter. Sgdr: Stochastic gradient descent with warm restarts. *arXiv preprint arXiv:1608.03983*, 2016.
- [56] David Zhang, Fengxi Song, Yong Xu, and Zhizhen Liang. *Feature Level Fusion*. Advanced Pattern Recognition Technologies with Applications to Biometrics, 2009.
- [57] David Zhang, Fengxi Song, Yong Xu, and Zhizhen Liang. Decision level fusion. In *Advanced pattern recognition technologies with applications to biometrics*, pages 328–348. IGI Global, 2009.
- [58] Yong Xu and Yuwu Lu. Adaptive weighted fusion: a novel fusion approach for image classification. *Neurocomputing*, 168:566–574, 2015.
- [59] Yimian Dai, Fabian Gieseke, Stefan Oehmcke, Yiquan Wu, and Kobus Barnard. Attentional feature fusion. In *Proceedings of the IEEE/CVF winter conference on applications of computer vision*, pages 3560–3569, 2021.
- [60] Ruibing Hou, Hong Chang, Bingpeng Ma, Shiguang Shan, and Xilin Chen. Cross attention network for few-shot classification. *Advances in neural information processing systems*, 32, 2019.